Earth and Planetary Science Letters 285 (2009) 75–86

Contents lists available at ScienceDirect

Earth and Planetary Science Letters

journal homepage: www.elsevier.com/locate/epsl

Shallow and deep crustal control on differentiation of calc-alkaline and tholeiitic magma

John M. Hora [a,*], Brad S. Singer [a], Gerhard Wörner [b], Brian L. Beard [a], Brian R. Jicha [a], Clark M. Johnson [a]

[a] Department of Geoscience, University of Wisconsin–Madison, 1215 W. Dayton Street, Madison, WI 53706, USA
[b] Geowissenschaftliches Zentrum der Universität Göttingen, Abteilung Geochemie, Goldschmidtstr. 1, 37077 Göttingen, Germany

ARTICLE INFO

Article history:
Received 10 December 2008
Received in revised form 26 May 2009
Accepted 27 May 2009
Available online 4 July 2009

Editor: R.W. Carlson

Keywords:
Parinacota
Andes
^{238}U–^{230}Th isotopes
$^{87}Sr/^{86}Sr$
lower crust
assimilation

ABSTRACT

The role of changing crustal interaction and plumbing geometry in modulating calc-alkaline vs. tholeiitic magma affinity is well illustrated by the influence of 70 km thick crust beneath Volcán Parinacota. Changes in petrologic affinity correlate with periods of cone-building, sector collapse, and rebuilding of the volcano over the last 52 ka, and are well explained by changes in magma recharge regime. With increasing recharge and magma output, lavas transition from low-Fe, strongly calc-alkaline, phenocryst-rich silicic compositions to medium-Fe, near-tholeiitic, mafic, and aphanitic characteristics. Strontium isotope data show that the change in magma regime did not affect all parts of the system simultaneously; these are characterized by distinctive $^{87}Sr/^{86}Sr$ ratios, which suggest an initially compartmentalized system. Relatively high ($^{230}Th/^{232}Th$) activity ratios of ~0.72 in early-erupted calc-alkaline lavas are consistent with interaction with high-U upper crust. Low ($^{230}Th/^{232}Th$) activity ratios of ~0.55 and up to 33% Th-excess in younger near-tholeiitic lavas correlate with steep REE patterns, indicating lower-crustal interaction. Thorium-excesses at the time of eruption approach the maximum that can be generated via small-degree garnet-residual melting in the lower crust or mantle and imply that transit time through the crustal column for the most tholeiitic magmas had to be short, on the order of $<2\times10^4$ yr. In contrast, lavas with greatest calc-alkalinity are also at or near secular equilibrium, suggesting stagnation times $>3\times10^5$ yr in the upper crust. In addition to more traditional explanations tied to magma source, expression of low-Fe 'calc-alkaline' (CA) vs. medium-Fe 'near-tholeiitic' (TH) magma series at the scale of individual volcanoes is likely to be modulated by transitions from compartmentalized, stagnant, assimilation-prone 'dirty' systems (CA) to 'clean' systems (TH) that are characterized by rapid magma throughput and minimal opportunity for upper-crustal contamination.

1. Introduction

Continental crust that overlies subduction zones filters magmas according to their density, and in most cases, passage through it modifies melt chemical and isotopic compositions. Evidence of magma–crust interaction has long been recognized in many arcs, and where crustal thickness varies along strike, the intensity of chemical modification co-varies with thickness (Leeman, 1983; Hildreth and Moorbath, 1988; Tormey et al., 1991). Where crust is heterogeneous, individual domains impart their isotopic fingerprints on transient magmas (Wörner et al., 1992; Kersting et al., 1996; Mamani et al., 2008). Stagnation that results in chemical modification may occur at two broadly defined locations: the base of the crust (Hildreth and Moorbath, 1988; Annen et al., 2006), and at shallow levels in plumbing systems that feed individual volcanoes. Here, we aim to discriminate the effects of shallow and deep assimilation and show how their relative importance varies over time.

Continental arcs challenge simple models for magmatic evolution because magmas with significant compositional, density, and rheological variability are commonly juxtaposed in such settings and it remains unclear why some magmas are filtered by the crust and others are not. Several models propose mechanisms whereby high-Fe (tholeiitic) vs. low-Fe (calc-alkaline) trends arise (Miyashiro, 1974; Arculus, 2003). Coulon and Thorpe (1981) and Leeman (1983) observed that the proportion of calc-alkaline magmas increases with crustal thickness. Experimental evaluation of closed-system thermodynamic controls on differentiation showed that calc-alkaline trends reflect high water contents and pressures that destabilize plagioclase and other silicates relative to oxides (Sisson and Grove, 1993). Moreover, increased pressure removes the thermal divide that otherwise suppresses calc-alkaline differentiation at low pressure (Grove and Baker, 1984; Grove and Kinzler, 1986). Assimilation of eutectic melts is an alternate, open-system mechanism where shallow systems can produce calc-alkaline magmas. Structural control of assimilation has been proposed to occur both on fine scales–in which local crustal thickness and stress regime determine magma–crust interaction (Kay et al., 1982)–and at regional scales of magmatic arcs where configuration of the subduction zone determines magmatic character (Portnyagin and Manea, 2008).

* Corresponding author. Tel.: +1 608 262 8960; fax: +1 608 262 0693.
E-mail address: jhora@geology.wisc.edu (J.M. Hora).

0012-821X/$ – see front matter © 2009 Elsevier B.V. All rights reserved.
doi:10.1016/j.epsl.2009.05.042

An important component to understanding magmatic evolution lies in the temporal control of open-system processes in a maturing arc system. Myers et al. (1985) advocate thermal maturation of the lithospheric conduit as a mechanism for generating calc-alkaline magmas, where magmas that stall and undergo extensive contamination produce "dirty" calc-alkaline differentiation trends, whereas high-magma fluxes coupled with short crustal residence times tend to favor "clean" tholeiitic differentiation. The Myers et al. (1985) model implies that differences between adjacent volcanoes are due to variably mature plumbing systems, rather than a consequence of variable crustal structure or thickness. Here we test the hypotheses that (1) degree of Fe-enrichment is a function of time and changing locus of magma–crust interaction, (2) phase equilibria mechanisms are of subordinate importance relative to upper-crustal assimilation in producing the wide array of Fe-enrichment observed in continental arc magmas, and (3) pseudo-trends that do not correspond to experimentally determined cotectics result from mixing of these variably Fe-enriched magmas.

Depth and elapsed time since magma–crust interaction are reflected in rare-earth element (REE), U, and Th elemental fractionations and resulting ^{238}U–^{230}Th systematics, respectively. These elements are fractionated by garnet, which is residual during deep crustal assimilation and can be a stable liquidus phase during high-P crystallization (Macpherson et al., 2006). Accordingly, increased REE and U–Th fractionation correlates with continental lithospheric thickness (Hildreth and Moorbath, 1988; Kay et al., 1999; Macpherson, 2008) and Garrison et al. (2006) proposed thickened crust as the explanation for ^{230}Th-excesses in continental arc magmas, which contrasts with the ^{238}U-excesses that are prevalent in island arcs (Turner et al., 2003).

U-series isotopes track time since fractionation (i.e., melting) and have been used to demonstrate instances of both rapid wedge-to-surface transit (Turner et al., 2001) and $>10^5$ yr of magma ponding prior to differentiation and eruption (Jicha et al., 2005) in island arcs. George et al. (2004) found that time scales of magmatic evolution were similar and short at Akutan (tholeiitic) and Aniakchak (mainly calc-alkaline) systems in the Aleutian arc, but that differentiation was more efficient in the calc-alkaline system. Transit times for continental arc magmas erupted through thicker crust, in general, appear to be longer, where any ^{238}U- and ^{226}Ra-excesses produced during melt generation has decayed to secular equilibrium by the time of eruption (Reagan et al., 2003). If magmas ascend through continental crust more slowly than in island arcs because of lower average continental crust densities, understanding of how, where, and for how long magmas stagnate within the crustal column is incomplete.

Here, we aim to distinguish chemical and U–Th isotope characteristics that arise primarily through deep vs. shallow crustal interaction, and gauge how the pace of magma ascent and recharge rates into the shallow magma reservoirs change over time. We take advantage of differences in ($^{230}Th/^{232}Th$) between lower and upper-crustal rocks to resolve the depth of interaction, and use the degree of secular disequilibrium to constrain time since deep crustal assimilation. We reconcile variable Fe-enrichment (i.e. tholeiitic vs. calc-alkaline character) with changing storage depths and differing rates of transport through the crust. Instead of comparing volcanoes along a segment of arc as is widely done (Myers et al., 1985; Hildreth and Moorbath, 1988; Kersting et al., 1996; Portnyagin and Manea, 2008), we focus on a single well-dated arc volcano on thick crust that changed from calc-alkaline to near-tholeiitic compositions during its history. New major- and trace-element data, U–Th, and Sr isotope data for lavas at Volcán Parinacota (N. Chile) that have been dated by $^{40}Ar/^{39}Ar$ (Hora et al., 2007) provide a high-resolution time-series of chemical and isotopic data that link edifice evolution, changing configuration of the magma reservoir, and variable magma source.

2. Geological setting and volcanology overview

Volcán Parinacota, a 46 km^3 Pleistocene–Holocene stratocone in the Andean Central Volcanic Zone (CVZ — Fig. 1 inset) was chosen for this study because of its location atop 70 km thick Precambrian continental crust (Beck et al., 1996; Yuan et al., 2002), which maximizes opportunity for crustal interaction. Variability in composition and age of crustal materials encountered at different depths are expected to impart distinct chemical and isotopic signatures to magmas comprising successive stages of volcano growth. Furthermore, detailed knowledge of Parinacota's eruptive chronology, extensive mapping at the resolution of individual lava flows, and thorough sampling of all major eruptive phases enable evaluation of chemical and textural changes over time.

2.1. Thick CVZ crust and its role in determining magma chemistry

The presence of thick crust imposes spatial and depth constraints on the mantle wedge material available for melting. Because the slab depth is similar to other arcs, the height of the asthenospheric wedge is reduced to ~30 km (Allmendinger et al., 1997); no part of it is shallow enough to be in the spinel-peridotite field (Robinson and Wood, 1998) as would be the case in island arcs, and therefore any wedge melting in the CVZ likely occurs in the presence of residual garnet. Thick crust also suggests garnet stability at the rheological and density boundaries comprising the base of the lithosphere and crust, respectively; we expect that partial melts sourced from the base of the CVZ crust and melts crystallizing there would show evidence of garnet-residual processes (Lee et al., 2006).

CVZ crust is compositionally diverse both laterally and vertically, however sparse basement exposure and extensive young volcanic and sedimentary cover preclude direct assessment of mid- and lower-crustal composition and structure. Lateral variation has been gauged via isotopic compositions of volcanic rocks, which reflect vertically integrated composition and age of underlying basement (Wörner et al., 1992; Aitcheson et al., 1995; Mamani et al., 2008). Parinacota is located within the Arequipa crustal domain (Ramos, 2008), where contaminated magmas are characterized by relatively unradiogenic Pb, low ε_{Nd} values, and elevated $^{87}Sr/^{86}Sr$ ratios from 0.706 to 0.708 (Mamani et al., 2008). Correlation between 3-D density structure and inferred chemical domains indicates that the proportion of mafic lower-crustal rocks to felsic upper-crustal lithologies is relatively high beneath the Arequipa domain (Mamani et al., 2008).

Vertical variation near Parinacota consists of unknown lower-crustal lithologies, mid-crust constrained by limited outcrops of metamorphic basement, and a veneer of Cenozoic volcanic and volcaniclastic rocks, sediments sourced largely from them, and their intrusive equivalents at depth. Because all of these units are significantly older than the half-life of ^{230}Th and have a wide range in U/Th ratios, this translates into a large spread along the equiline that distinguishes each of the potential assimilants. Paleozoic amphibolite and gneiss exposed ~40 km to the west at Belén, and mid-Proterozoic granulite and charnockite ~50 km to the east at Cerro Uyarani (Wörner et al., 2000b) both have low $^{206}Pb/^{208}Pb$, suggesting long-term depletion of U/Pb and U/Th ratios. These low U/Th ratios correspond to secular equilibrium activity ratios for ($^{238}U/^{232}Th$) and ($^{230}Th/^{232}Th$) of ~0.4–0.5 (Bourdon et al., 2000; Wörner et al., 2000b). Basement rocks from S. Peru have ($^{238}U/^{232}Th$) and ($^{230}Th/^{232}Th$) as low as 0.2 (Mamani et al., in press). In contrast, Cenozoic volcanic rocks that include the 22.7–19.4 Ma Oxaya Ignimbrites and 2.7 Ma Lauca-Perez Ignimbrite (Wörner et al., 2000a) have secular equilibrium activity ratios of ~0.7 and 1.0, respectively. Because the inferred source of the Lauca-Perez Ignimbrite is ~15 km to the northwest of Parinacota (Wörner et al., 2000a), recycling of its solidified intrusive equivalents by Parinacota magmas is possible.

2.2. Volcano evolution and unit descriptions

We focus on the last 52 ka of the 163 ka volcanic history at Parinacota (Hora et al., 2007) because (1) following a significant hiatus, the magma reservoir operated continuously during this time and was sampled frequently by eruption, and (2) the succession of

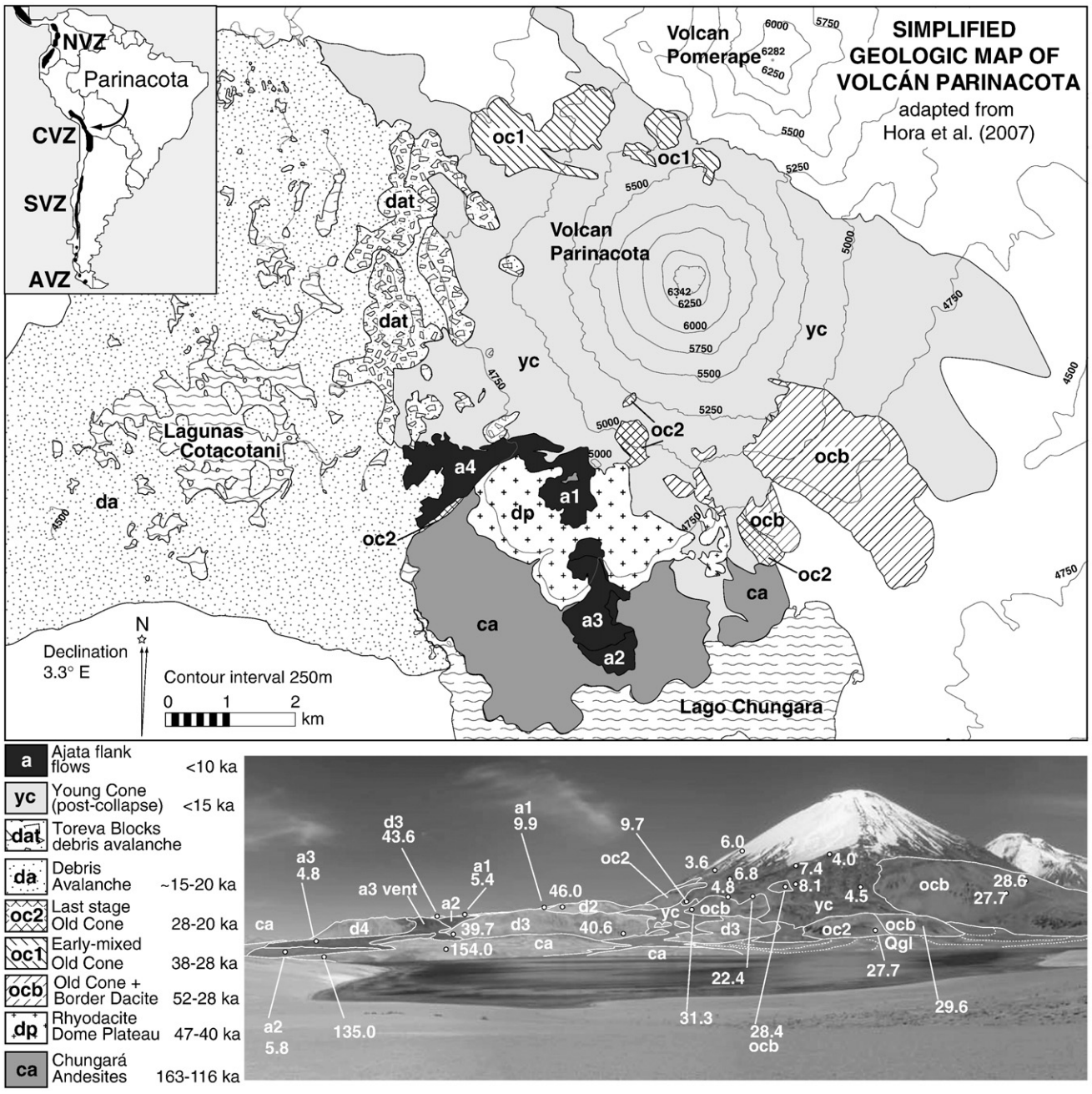

Fig. 1. Simplified geologic map and morphological evolution of Parinacota Volcano, unit ages from Hora et al. (2007). Parinacota units overlie the adjacent Pomerape edifice and Chungará andesites (*ca*). Following a 65 ka hiatus, several magma types were concurrently erupted in the earliest phase of the old cone: *occ* — sparsely porphyritic dacties from the northern portion of the old cone, *dp* — porphyritic rhyodacites of the dome plateau that underlie the southern part of the edifice, and cone-building andesites (*oc1* — 47–37 ka and *oc1a* — 33–28 ka). In the time interval 31–28 ka, voluminous eruptions (~3 km^3) of the 'border dacite' (*ocb*) built much of the south flank of the old cone. Old cone history since 28 ka is represented by andesitic lavas that contain variable amounts of phenocrysts (cpx-andesites through plag-amphibole-andesites; *oc2* — 28–22 ka). After sector collapse, the basaltic andesitic–andesitic young cone (*yc* — sampled interval 8 ka to present) formed a conical edifice that masks the sector collapse scar. Most recently, a series of Ajata flank vents (*a1*, *a2*, *a3*, and *a4* — 10–2 ka) erupted the most primitive lavas on the volcano (53–59% SiO_2).

erupted compositions suggests correlation between evolution of the edifice and change in reservoir processes. Initially (52–28 ka) a number of small, spatially separated centers with distinct composition (*dp*, *occ*, *ocb*, *oc1*, *oc1a* — Fig. 1) amalgamated to form an 'old cone' edifice (*oc2* — 28–20 ka). Successively erupted magma batches are more mafic than their predecessors, necessitating an open-system (mixing) model (Wörner et al., 1988). The old cone collapsed between 20 and 15 ka (Hora et al., 2007), forming a 6 km^3 debris avalanche deposit (Clavero et al., 2002). Unlike Mt. St. Helens, sector collapse at Parinacota apparently was not accompanied by eruption of juvenile material, but was followed by rapid building of a young cone (*yc*). Most post-collapse lavas have relatively homogenous major-element composition and erupted from the central vent, forming a symmetrical cone; however, a volumetrically small subset of these lavas erupted from flank vents (Ajata flows) have distinct trace-element composition. These flank lavas can not be related to each other by crystal fractionation, nor can they be directly parental to the evolved lavas of the old cone (Davidson et al., 1990).

Composition of mafic inputs is obscured in homogenized melts erupted from the young cone summit vent (*yc*), however flank Ajata flows (*a1*, *a2*, *a3*, and *a4*) have more diverse trace-element compositions indicative of their origin. Strontium and Ba concentration (hereafter noted as [Sr] and [Ba]) are particularly variable among the Ajata flows; unit *a3* has anomalously high [Sr] and [Ba] relative to other CVZ

magmas. Zoned plagioclase in mixed pre-collapse lavas (Ginibre et al., 2002; Ginibre and Wörner, 2007) records presence of both high-[Sr, Ba] and low-[Sr, Ba] melts during crystal growth. These two contrasting Ajata compositions have been identified as mixing endmembers for recharge during the entire history of Parinacota (Ginibre and Wörner, 2007). Entenmann (1994) showed using $^{87}Sr/^{86}Sr$ and $\delta^{18}O$ that both types of Ajata magma incorporated ~15% crustal material. Recharge-assimilation-fractionation-tapping (RAFT) modeling of trace-element variations indicate that high-[Sr, Ba] magma interacted at a deeper crustal level, where garnet was the only fractionating aluminous phase, whereas the low-[Sr, Ba] magma additionally fractionated plagioclase at shallower depth (Entenmann, 1994). Bourdon et al. (2000) were first to show that ($^{230}Th/^{238}U$) correlates with La/Yb and Ba/Hf ratios, indicating that trace-element fractionation is of recent origin.

3. Sample selection and analytical techniques

Major- and trace-element contents and Sr isotope compositions are presented in Supplemental File 1 for all 57 samples that have been dated using $^{40}Ar/^{39}Ar$ geochronology (Hora et al., 2007). Thirty-two samples representative of all major stages of volcano evolution were analyzed for ^{238}U–^{230}Th isotopes (Table 1), and can be correlated to a more extensive geochemical dataset from previous studies (Wörner et al., 1988; Davidson et al., 1990). Field methods, stratigraphic context of samples, and a detailed map can be found in Hora et al. (2007). Sample preparation and analytical methods for all major-element analyses (XRF), trace-element analyses (quadrupole ICP-MS), Sr isotope measurements (TIMS) and U–Th isotope measurements (MC-ICP-MS) are given in Supplemental File 2.

4. Results

Below we first cast the results in terms of a calc-alkaline (CA) and tholeiitic (TH) index to highlight distinct petrologic affinities that are mirrored in trace-element and isotopic data. Both short- and long-term trends in chemical and isotopic compositions are then placed in the context of spatial relations on the volcano and in the region.

4.1. CA/TH index and its use

All Parinacota magmas are calc-alkaline, but their degree of Fe-enrichment at a given silica content varies (Fig. 2). Recognizing that a

Table 1
Summary of U–Th data from Parinacota Volcano lavas.

Sample[a]	Unit	$^{40}Ar/^{39}Ar$ Age[b] (ka)	n[c]	Th (ppm)	U (ppm)	($^{238}U/^{232}Th$)	($^{230}Th/^{232}Th$)	($^{230}Th/^{232}Th)_0$[d]	($^{230}Th/^{238}U)_0$[d]
Ajata flows									
PAR-03-25	*a4*	2.6 ± 1.3	1	7.830	1.354	0525 ± 0.011	0.560 ± 0.004	0.561 ± 0.004	1.069 ± 0.023
PAR-201	*a4*	2.6 ± 1.3	2	7.867	1.342	0.518 ± 0.003	0.558 ± 0.003	0.559 ± 0.003	1.079 ± 0.008
PAR-03-21	*a3*	4.8 ± 4.0	2	8.389	1.195	0.432 ± 0.002	0.545 ± 0.003	0.550 ± 0.005	1.272 ± 0.014
PAR-220	*a2*	5.8 ± 7.4	2	6.129	1.701	0.842 ± 0.005	0.709 ± 0.004	0.702 ± 0.010	0.834 ± 0.013
PAR-03-20	*a1*	5.4 ± 2.7	2	7.814	1.314	0.510 ± 0.003	0.558 ± 0.003	0.561 ± 0.003	1.099 ± 0.009
PAR-03-19	*a1*	9.9 ± 2.1	2	7.702	1.308	0.515 ± 0.007	0.562 ± 0.010	0.567 ± 0.010	1.101 ± 0.026
Young cone									
PAR-03-43	*yc*	0.5 ± 0.3	2	6.774	0.988	0.442 ± 0.006	0.581 ± 0.003	0.581 ± 0.003	1.314 ± 0.020
PAR-03-39	*yc*	3.6 ± 1.1	1	8.385	1.411	0.510 ± 0.010	0.559 ± 0.004	0.561 ± 0.004	1.099 ± 0.024
PAR-03-14	*yc*	4.0 ± 1.2	1	8.300	1.388	0.507 ± 0.010	0.562 ± 0.004	0.564 ± 0.004	1.112 ± 0.024
PAR-04-09	*yc*	4.5 ± 3.0	1	7.600	1.135	0.453 ± 0.009	0.569 ± 0.004	0.573 ± 0.005	1.265 ± 0.029
PAR-03-15	*yc*	4.6 ± 2.6	1	7.396	1.101	0.452 ± 0.009	0.567 ± 0.004	0.572 ± 0.005	1.267 ± 0.028
PAR-04-12	*yc*	4.8 ± 0.8	1	9.402	1.615	0.521 ± 0.010	0.592 ± 0.004	0.595 ± 0.004	1.142 ± 0.025
PAR-03-38	*yc*	6.0 ± 3.4	1	7.582	1.128	0.452 ± 0.009	0.562 ± 0.004	0.568 ± 0.006	1.259 ± 0.029
PAR-03-34	*yc*	6.8 ± 3.2	1	6.833	0.990	0.439 ± 0.009	0.578 ± 0.004	0.587 ± 0.006	1.336 ± 0.031
PAR-04-10	*yc*	8.1 ± 1.8	1	7.655	1.146	0.454 ± 0.009	0.564 ± 0.004	0.573 ± 0.005	1.262 ± 0.029
Old cone									
PAR-04-13	*oc2*	22.4 ± 7.5	3	8.879	1.368	0.467 ± 0.005	0.566 ± 0.002	0.588 ± 0.009	1.260 ± 0.026
PAR-03-28	*oc2*	22.9 ± 6.3	1	10.106	2.154	0.647 ± 0.013	0.681 ± 0.005	0.688 ± 0.007	1.064 ± 0.028
DBF-03-05	*oc2/da*	23.0 ± 3.5	1	11.549	2.537	0.667 ± 0.013	0.683 ± 0.005	0.687 ± 0.007	1.030 ± 0.027
PAR-03-05	*ocb*	27.7 ± 1.6	4	11.349	2.640	0.706 ± 0.007	0.714 ± 0.003	0.716 ± 0.004	1.015 ± 0.014
PAR-03-36	*oc2*	27.9 ± 4.3	1	11.490	2.644	0.698 ± 0.014	0.711 ± 0.005	0.714 ± 0.008	1.023 ± 0.028
PAR-03-09	*oc1a*	28.4 ± 3.7	1	8.262	1.718	0.631 ± 0.013	0.647 ± 0.005	0.652 ± 0.007	1.033 ± 0.028
DBF-03-04	*oc1a/da*	29.2 ± 4.5	1	8.840	1.910	0.656 ± 0.013	0.666 ± 0.005	0.669 ± 0.007	1.021 ± 0.028
DBF-03-03	*oc1a/da*	31.8 ± 6.6	1	8.587	1.826	0.645 ± 0.013	0.659 ± 0.005	0.664 ± 0.008	1.029 ± 0.029
PAR-03-11	*oc1*	37.8 ± 6.8	1	10.442	2.164	0.629 ± 0.013	0.671 ± 0.005	0.688 ± 0.009	1.095 ± 0.033
DBF-03-09	*occ/da*	45.2 ± 1.9	1	13.143	3.023	0.698 ± 0.014	0.698 ± 0.005	0.699 ± 0.010	1.001 ± 0.032
PAR-03-10	*oc1*	46.7 ± 1.6	2	12.879	2.785	0.656 ± 0.009	0.685 ± 0.015	0.701 ± 0.024	1.068 ± 0.042
Dome Plateau									
PAR-03-17	*du/da*	29.4 ± 6.1	1	26.178	7.451	0.864 ± 0.007	0.810 ± 0.006	0.793 ± 0.009	0.918 ± 0.014
PAR-04-02	*d3*	39.7 ± 1.9	1	19.734	4.668	0.718 ± 0.006	0.716 ± 0.005	0.715 ± 0.008	0.996 ± 0.015
PAR-03-18	*d2*	43.6 ± 2.4	5	18.975	4.514	0.721 ± 0.005	0.724 ± 0.002	0.725 ± 0.004	1.005 ± 0.010
DBF-03-06	*du/da*	45.3 ± 5.8	1	30.246	7.914	0.794 ± 0.006	0.781 ± 0.006	0.774 ± 0.009	0.974 ± 0.016
PAR-03-26	*d1*	47.0 ± 1.3	2	16.609	3.888	0.710 ± 0.005	0.718 ± 0.004	0.722 ± 0.006	1.016 ± 0.014
Chungará andesites									
PAR-03-31	*ca*	162.9 ± 8.9	1	9.146	1.651	0.548 ± 0.011	0.580 ± 0.004	0.692 ± 0.044	1.264 ± 0.103

All analytical uncertainties reported at 2σ precision, external reproducibility based on replicate standard and sample analyses.
Decay constants used for activity calcualtions: ^{238}U, 1.5513×10^{-10}/yr; ^{230}Th, 9.1577×10^{-6}/yr (Cheng et al., 2000); ^{232}Th, 4.948×10^{-11}/yr.

[a] Additional information (i.e. major and trace element compositions and Sr isotopic ratios, as well as full U–Th results) for these samples can be found in Tables 1, 2, and Supplementary data in the online version.

[b] Data from Hora et al. (2007). Methods, calcualtion of uncertainties and criteria for determining preferred ages can be found therein.

[c] n refers to the number of Th analyses clone on a particular sample. For $n>1$, tabulated values are weighted averages reported with their corresponding uncertainties.

[d] Eruption age-corrected initial activity ratios incorporate uncertainty in $^{40}Ar/^{39}Ar$ age.

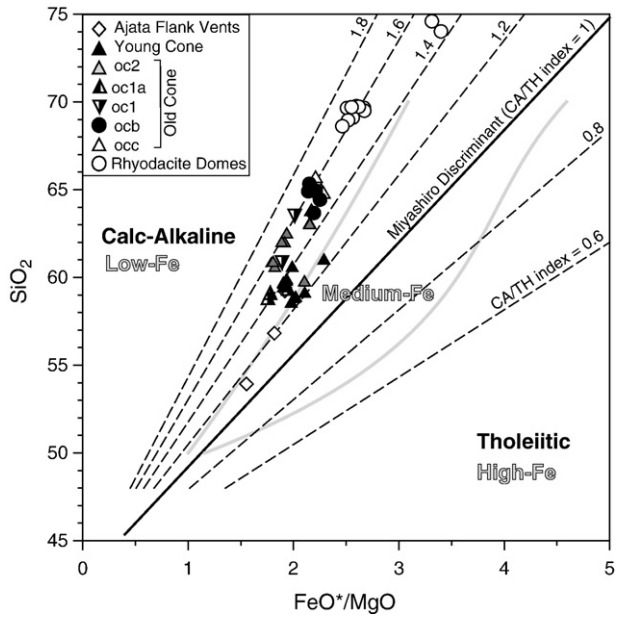

Fig. 2. Plot of Parinacota differentiation series relative to calc-alkaline and tholeiitic fields of Miyashiro (1974) and high-, medium- and low-Fe fields of Arculus (2003). Dashed lines indicate uniform CA/TH index. Old cone lavas that contain >62 wt.% SiO_2 and dome plateau lavas have CA/TH indices that range from 1.4 to 1.7. In contrast, young cone and Ajata lavas have CA/TH indices between 1.1 and 1.4. The transition between these trends occurred within lavas erupted in the later portion of old cone history.

continuum exists between tholeiitic and calc-alkaline trends, Arculus (2003) proposed divisions of low-, medium-, and high-Fe magmas, corresponding to calc-alkaline, transitional, and tholeiitic magmas using the nomenclature of Miyashiro (1974). To quantify the degree to which a particular magma is a result of mixing among trends of tholeiitic or calc-alkaline character, we define:

$$\text{CA/TH index} = (\text{wt.\%SiO}_2 - 42.8) / (6.4 \times \text{FeO*/MgO})$$

which is tied to the ratio of slopes on a SiO_2 vs. FeO*/MgO plot (Miyashiro, 1974). At any SiO_2 content, magmas belonging to a trend that has CA/TH index >1 are calc-alkaline; higher indices therefore correspond to trends of lower relative Fe-enrichment. For systems controlled only by fractional crystallization, CA/TH index should remain nearly invariant. At Parinacota, CA/TH indices remained nearly invariant prior to 28 ka, but graded toward tholeiitic affinity in successively more mafic magmas that built the later portion of the old cone, young cone, and Ajata flows.

4.2. Long-term morphologic, chemical, and isotopic changes through time

Several parameters co-vary with the CA/TH index over the history of Parinacota (Fig. 3a). Erupted volumes were sub-equal for old and young cones, however eruptive rate increased throughout Parinacota history (Fig. 3b). ($^{230}Th/^{232}Th$) decreased (Fig. 3c), and the magnitude of U–Th secular disequilibrium increased as indicated by more variable ($^{238}U/^{230}Th$) with decreasing eruption age (Fig. 3d).

4.3. Short-term chemical and isotopic trends

Subordinate trends that lasted several ka are superimposed on long-term variations. Prior to 28 ka, large diversity in SiO_2 content existed (Fig. 3e) but $^{87}Sr/^{86}Sr$ ratios during this time period formed three distinct groups, which in turn exhibit increasing, constant, and decreasing SiO_2 contents with time. Lavas comprising these groups are spatially separated on the volcano. The rhyodacite domes (*dp* — Figs. 1 and 3) have homogeneous $^{87}Sr/^{86}Sr$ ratios of 0.70676 ± 1 ($n = 10$) and variable $(^{230}Th/^{232}Th)_0$ from 0.715 to 0.725 within error of secular equilibrium. In this group, SiO_2 content increased and trace elements were uniform over time — [Sr] ≈ 600 ppm and [Ba] ≈ 1000–1200 ppm. The constant-SiO_2 group (*occ* and *ocb* — Fig. 3) has a restricted range in $^{87}Sr/^{86}Sr$ (0.70681 ± 2), $(^{230}Th/^{232}Th)_0$ varies from 0.699 to 0.716, is in U–Th secular equilibrium, has [Sr] ≈ 800 ppm, and [Ba] ≈ 1000–1200 ppm. In contrast, the group consisting of *oc1* and *oc1a* units (Fig. 3) in which SiO_2 contents decreased over time (62 to 57 wt.%, $n = 5$) has $(^{230}Th/^{232}Th)_0$ ratios (0.701–0.651) that are lower relative to coeval lavas described above and have small-degree Th-excess. Within this group, the earlier-erupted lavas (*oc1*) have $^{87}Sr/^{86}Sr = 0.70662$, higher [Sr] = 1100 ppm and [Ba] = 1300 ppm; the later-erupted lavas (*oc1a*) have higher $^{87}Sr/^{86}Sr = 0.70672 \pm 2$, but similar [Sr] and [Ba].

The time interval after eruption of large-volume dacite flows at 28 ka is characterized by scattered trends in chemical and isotopic data. In *oc2*, SiO_2 ranges between 57 and 62 wt.%, and $^{87}Sr/^{86}Sr$ varies between 0.70660 and 0.70681, with no correlation to other compositional parameters. $(^{230}Th/^{232}Th)_0$ and $(^{230}Th/^{238}U)$ for three analyzed samples in this group are highly variable (Fig. 3c–d). The lavas that compose the main edifice of the young cone are relatively homogenous in SiO_2 contents of 57.5–59.8 wt.%, as well as $(^{230}Th/^{232}Th)_0$ ratios of 0.561–0.595, but are variable with respect to [Sr] of 942–1108 ppm, $^{87}Sr/^{86}Sr$ of 0.70660–0.70681, and the degree of secular disequilibrium, where $(^{230}Th/^{238}U)_0$ varies from 1.099 to 1.336.

4.4. U–Th data and regional comparison

Despite eruption ages of <52 ka–much shorter than the half-life of ^{230}Th–many pre-collapse Parinacota lavas are within uncertainty of secular equilibrium. On an equiline diagram, U–Th data form an array (Fig. 4) between near-equiline dome plateau (*dp*) lavas with $(^{230}Th/^{232}Th) = 0.72$, and two clusters of young (post-collapse) lavas. These two groups are typified by *a1* and *a3* mixing endmembers as suggested by Ginibre and Wörner (2007): both have low $(^{230}Th/^{232}Th) = 0.55$ but differing amounts of Th-excess. The lower Ajata flow (*a2*) is distinct from all other post-collapse lavas because it has U-excess, and higher $(^{230}Th/^{232}Th)$. The overall range in $(^{230}Th/^{232}Th)$ is bracketed by lower-crustal and upper-crustal lithologies as discussed in Section 2.2.

5. Discussion

We focus on the depths and extent of crustal interaction as constrained by trace-element and isotopic data before discussing how involvement of magmas with various sources changed the magmatic system over its history. All data are confined to a mixing tetrahedron (Supplemental File 3) with apices defined by the chemical and isotopic compositions of the early-erupted dome plateau (*dp*), and Ajata lavas *a1*, *a2*, and *a3*. These three mafic endmembers erupted from flank vents are important because they are not polluted by mixing with magma that was resident in the shallow reservoir, and we interpret compositional variability to reflect different degrees and locations of partial melting within the crust. Combined REE and Th isotope, and major-element data suggest that the degree to which shallow contamination overprints the signature of deep crustal melting largely determines the calc-alkalinity of differentiated magmas. Even though mixing among endmembers undoubtedly needs to be considered in the interpretation of Th isotope data (see also Section 5.4), the extent of eruption-age-corrected Th isotope disequilibria of mafic lavas imposes time limits on magma storage and ascent.

5.1. Chemical signatures of deep processing

Steep REE patterns in Parinacota lavas which have chondrite-normalized $(La/Yb)_N$ ratios between 18 and 45 (Supplemental File 4), indicate involvement of garnet either as a residual phase during

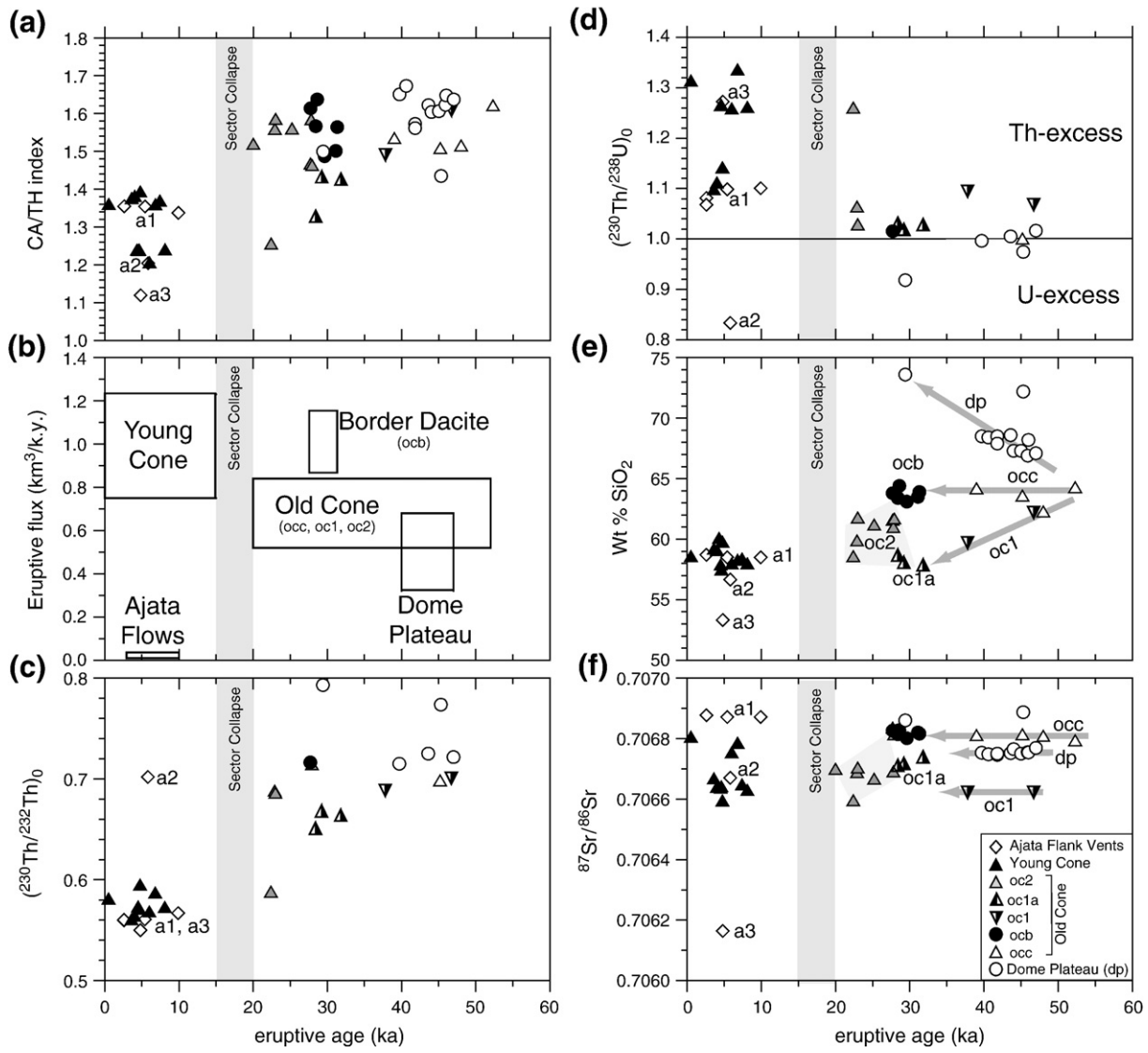

Fig. 3. Various chemical, isotopic, and mass flux parameters plotted vs. 40Ar/39Ar eruptive age (Hora et al., 2007) for Parinacota lavas. (a) CA/TH index indicates a decrease over time, however the decrease does not affect all parts of the system at the same time. (b) Eruptive flux through time. Box height indicates uncertainty in erupted volume, which translates into uncertainty in flux, and box width represents the time span during which lavas of that unit were erupted. (c) ($^{230}Th/^{232}Th$) ratio decreases with time. Outlier with ($^{230}Th/^{232}Th$) = 0.71 is Ajata lava *a2*, see also Section 5.2 of the text. (d) Most Old Cone lavas plot near the equiline whereas most Young Cone and Ajata lavas have Th-excess, with the exception of Ajata lava *a2* with U-excess. (e) Temporal variation in SiO_2 content. (f) Range in $^{87}Sr/^{86}Sr$ ratio is limited throughout the history of Parinacota. Prior to 28 ka, three batches of magma with uniform $^{87}Sr/^{86}Sr$ (gray arrows) correspond to coherent trends in SiO_2 with time.

melting or as a fractionating phase. Garnet-residual melting can occur over a wide range of depths in the CVZ, from the asthenospheric wedge to mid-crustal levels. Because water suppresses plagioclase crystallization and stabilizes both garnet and amphibole in the mid- to lower-crust (Muntener et al., 2001), deep hydrous arc magmas may also show evidence of liquidus garnet crystallization.

Detection of amphibole vs. garnet fractionation in the deep crust for a single melt batch has been demonstrated using Dy/Yb trends (Davidson et al., 2007), however deconvolution of the effects of garnet-residual melting can be problematic. Differences in mineral-melt partition coefficients (D) between amphibole ($D_{Dy} > D_{Yb}$) and garnet ($D_{Dy} \ll D_{Yb}$) result in opposite Dy/Yb trends in evolving melt. Volcanoes on thin crust tend to have well-constrained negative trends in Dy/Yb vs. SiO_2, indicating (1) amphibole fractionation and (2) relatively homogenous Dy/Yb in parental magmas. This is not the case for Parinacota, and most other volcanoes built on crust exceeding 40 km (Fig. 5). Positive trends indicative of garnet fractionation such as those in Surigao Peninsula (Philippines) lavas are rare (Macpherson, 2008). Because enrichment in incompatible elements is highly dependent on the melt fraction (F), small differences in degree of garnet-residual melting where F is small can have a disproportionately large effect on Dy/Yb, and can easily override the signal from fractional crystallization where F is large. At Parinacota, overall elevated Dy/Yb most likely result from garnet-residual melting and scatter caused by small differences in F during melting among magma batches impedes detection of a fractionation signal.

Correlation among La/Yb, Dy/Yb, and ($^{230}Th/^{238}U$) ratios in Ajata endmember samples indicates that degree of garnet-residual partial melting likely controls all three parameters (Supplemental File 5a,b) and that trace-element fractionation is of recent origin (Bourdon et al., 2000). A lack of correlation between La/Yb and CA/TH index (Supplemental File 5c) indicates that Mg/Fe ratios are not controlled by source processes. Instead, correlation of CA/TH with contamination indices (SiO_2, K_2O, and Cs — Supplemental File 5d–f) indicates that trends of variable CA/TH index are likely mixing lines, in which upper-crustal assimilation controls Mg/Fe ratio. Mixing may be responsible

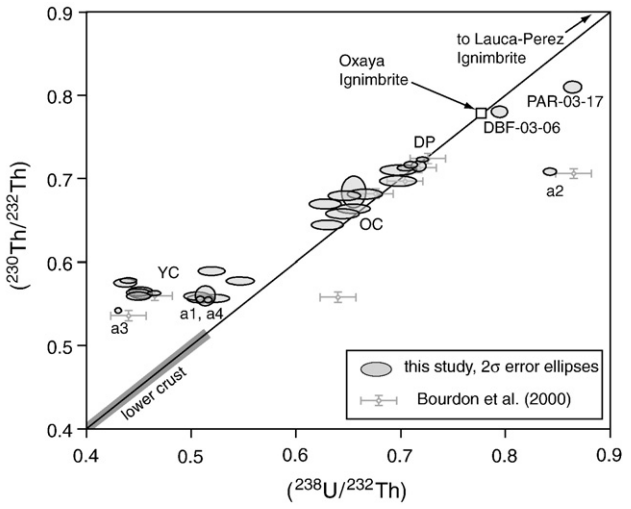

Fig. 4. Equiline diagram for Parinacota lavas. All lavas erupted prior to sector collapse have (^{230}Th/^{232}Th) >0.6, whereas lavas erupted after sector collapse have (^{230}Th/^{232}Th) <0.6. Post-collapse lavas form two groups with different (^{238}U/^{232}Th), corresponding to *a3* and *a1* Ajata compositions.

for the global prevalence of trends that cross from tholeiitic to calc-alkaline fields with increasing SiO_2 and the paucity of trends in the opposite direction.

5.2. Mantle and lower-crustal effects on U–Th disequilibrium

The REE evidence for interaction of Parinacota magmas with deep garnet-bearing crust bears on how U–Th isotope data are interpreted. Differences in (^{238}U/^{232}Th) activity ratios at similar (^{230}Th/^{232}Th) reflect differences in melting conditions that produced the parental magmas (Fig. 6a). Fluid-mobile U carried from the subducting slab into the mantle wedge will produce U-excess (Allegre and Condomines, 1982) and flank eruption *a2* is inferred to have partially retained such a mantle-derived signature. The near-equiline high (^{230}Th/^{232}Th) magmas of the dome plateau (*dp*) endmember also suggest a parental melt with initial U-excess and subsequent decay to secular equilibrium, assuming similar mantle wedge U–Th ratios as post-collapse lavas. In contrast, most post-collapse lavas (*a1*, *a3*, and *yc*) have Th-excesses. Because CVZ mantle melts are sourced entirely within the garnet peridotite stability field, the degree of U-excess may be reduced relative to that inherited from slab fluids. Both U and Th are incompatible in mantle minerals, and thus >10% partial melting results in ^{230}Th-excesses of only ~2%. Similarly, fractional crystallization of garnet, where $D_U/D_{Th} \gg 1$ produces Th/U-excess only at unrealistically high degrees of crystallization (>99%); neither large degree partial melting in the mantle wedge nor moderate amounts of crystallization are viable mechanisms for producing the large Th-excess observed in young cone and Ajata lavas, and is consistent with high Dy/Yb.

Small degrees of partial melting of garnet-bearing lithologies are required to explain the Th-excesses at Parinacota because only under these conditions is Th fractionated from U to a sufficient degree. Even so, 1 and 2% batch partial melts of Belen garnet biotite gneiss (5% garnet) initially at secular equilibrium will generate 14 and 7% Th-excess, respectively (Table 2). To produce observed Th-excesses, a putative lower-crustal lithology with higher garnet mode is required. Batch melting of garnet pyroxenite (25% garnet) at 1 and 2% melt fractions, produces 29 and 19% Th-excess, respectively (Table 2). The above models are a highly simplified case: Th-excess depends on the proportion of garnet, which largely controls bulk *D*, as well as the choice of mineral partition coefficients used. Determinations of D_U/D_{Th} ratios in garnet of various compositions vary from 1.3 to 9.3 (e.g., van Westrenen et al., 1999; Pertermann et al., 2004), but most are within the range of 3–6. Here, we use partition coefficients of Elkins et al. (2008) for garnet which yield $D_U/D_{Th} = 4.06$. We use partition coefficients of Wood et al. (1999) for clinopyroxene because they account for greater U compatibility at high pressure, and those of Blundy and Wood (2003) for other phases.

Dynamic mantle melting models show that: (1) decreased melting rates result in ingrowth of ^{230}Th in the unmelted portion of the source prior to melt separation (Williams and Gill, 1989; Zou and Zindler, 2000), and (2) decreased porosity in the melting region (Zou and Zindler, 2000) can fractionate Th from U enough to increase (^{230}Th/^{238}U) activity ratios by 5–15%. Similarly, we envision that melting at several levels in the lower- and mid-crust, may increase Th/U fractionation relative to simple batch models. If operating continuously, this is analogous to zone-refining concentration of Th relative to U in the melt as it migrates through the crust.

We anticipate that melt which exited the melting-assimilation-storage-homogenization (MASH) zone was a hybrid made up of mantle and crustal melts (Fig. 6a). Trace-element and isotopic modeling of *a2* and *a3* lavas by Entenmann (1994) inferred a 6:1 ratio of mantle:crustal components. Because U and Th concentrations are relatively high in the small-degree crustal melts that are required to explain the large Th-excesses, such melts will dominate the U and Th budget of the resulting mixture. Therefore, Th/U ratios in the hybrid melt are relatively insensitive to the degree of initial U-excess in the mantle melt. For example, admixture of a mantle melt with 20% U-excess decreases Th-excess in crustal melt by only ~2–4%. These considerations indicate that Th-excesses in Parinacota magmas are relatively independent of the characteristics of the mantle component involved, and may be confidently ascribed to lower-crustal melting processes involving garnet-bearing rocks.

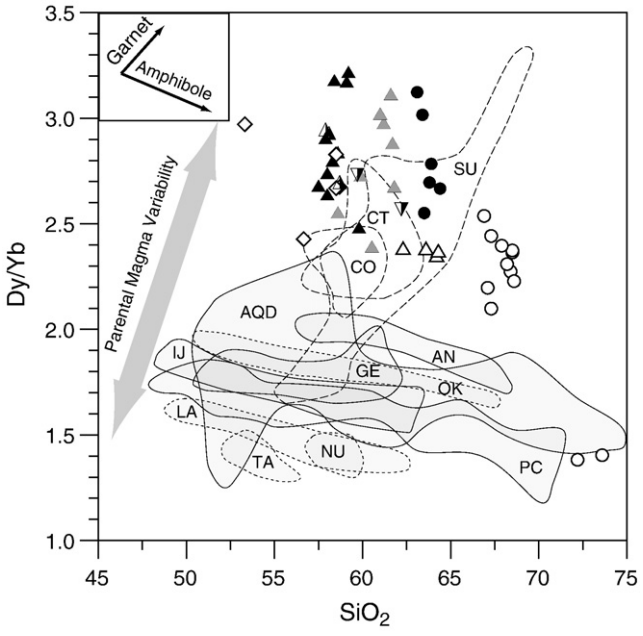

Fig. 5. Dy/Yb vs. SiO_2 plot after Davidson et al. (2007) with Parinacota data plotted, symbols as in Figs. 2 and 3. Fields indicate data ranges for other extensively studied volcanoes, and data are from Davidson et al. (2007) unless otherwise noted. Island arcs = short-dashed fields: TA = Tafahi (Tonga), NU = Nuia (Tonga), OK = Okmok, LA = Lesser Antilles (encompassing overlapping fields for St. Kitts, Quill, and Pelee). Continental arcs = solid lined fields: IJ = Ijen (Java), GE = Gede (Java), AN = Aniakchak, PC = Puyehue–Cordon Caulle – SVZ, 40.5°S (Singer et al., 2008), AQD = Cerro Azul, Quizapu, Descabezado Grande – SVZ, 35.5°S (Hildreth and Moorbath, 1988). Long-dashed fields indicate continental volcanoes: CT = Cerro Tupungato – SVZ, 33.5°S (Hildreth and Moorbath, 1988), CO = Cotopaxi (NVZ), SU = Surigao Peninsula (Philippines). Dy/Yb in parental compositions for trends correlates with increasing crustal thickness in single arcs, e.g. PC, AQD, and CT data from the Andean SVZ.

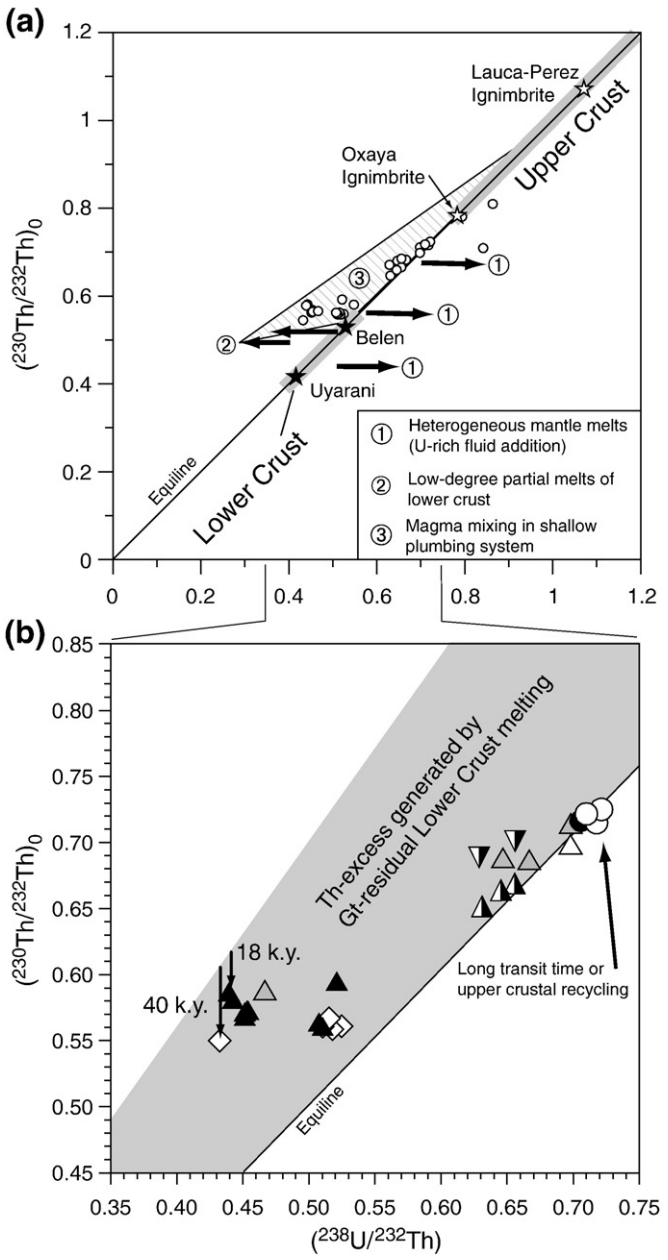

Fig. 6. (a) Schematic illustration of the effects of partial melting of various mantle and crustal lithologies. Fluid-fluxed partial melting of a heterogeneous mantle wedge results in U-excess melts that have (^{230}Th/^{232}Th) indicative of the mantle source (1). Partial melting of low (^{230}Th/^{232}Th) lower-crustal lithologies (filled stars) with residual garnet, initiated by underplating of (1) results in Th-excess, which is maximized by lower degrees of partial melting (2). Mixing of (1) and (2) results in hybrid melts that plot near (2) due to higher concentrations of both U and Th in (2) relative to (1). Partial melting of high (^{230}Th/^{232}Th) upper-crustal materials (e.g. ignimbrites, open stars) results in minimal U–Th fractionation. Mixing of upper-crustal near-equiline melts with hybrid melts (1 + 2) can result in an array (3) that is similar to variation observed in Parinacota data (open circle symbols). (b) Maximum Th-excess that can be produced by processes such as (2) is ~40% (gray shaded area). Starting from such maximum allowable amount of Th-excess to the eruption-age corrected Th-excess observed at Parinacota provides an upper limit on ascent times from the region of partial melting to the surface, e.g. 40 and 18 ka for two representative young cone samples. It is likely that true transit times were faster if parental Th-excess was smaller than the maximum amount (e.g. transit times for the two samples decrease to 27 and 6 ka, respectively, if parental Th-excess had been 35%). Unit symbols as in Fig. 2, symbol size is representative of average uncertainty.

5.3. Constraints on time since deep crustal partial melting

The magnitude of Th-excesses in post-collapse samples requires that elapsed time between lower-crustal interaction and eruption was short. Measured Th-excesses in the subset of young cone lavas that are similar to the *a3* component approach the maximum Th-excess that can be produced by crustal melting (Fig. 6). The bulk of global U–Th data from continental arcs has (^{230}Th/^{238}U) <1.2, but very few volcanoes, e.g. Mt. Adams (Jicha et al., 2009), have greater Th-excess than young cone lavas at Parinacota. Collectively, these data suggest that ~40% Th-excess represents a limiting case in terms of slow melting rates, low porosity, and small melt fractions derived from arc crust. Because eruption age-corrected Parinacota data are near this limit, maximum allowable crustal transit times are on the order of a few tens of ka (Fig. 6b).

In contrast, the origin of the silicic, near-equiline, high U/Th endmember in Fig. 6a, typified by the dome plateau lavas (*dp*) requires a different origin: either (1) assimilation of secular equilibrium upper-crustal material in absence of a garnet residue or (2) highly fractionated, old (>250 ka) magmas that had initial U-excess. If (1) is correct, and both the upper-crustal assimilant and the hybrid melt (*dp*) are on the equiline, then the input melt that initiated assimilation also must have been on the equiline. This would occur if the input melt either (case 1a) had no initial (^{230}Th/^{238}U) disequilibrium and may be young, or (case 1b) was initially in U-series disequilibrium, therefore requiring enough time to decay to secular equilibrium. If (2) is correct, and *dp* is a highly fractionated melt with initial U-excess (similar to *a2*), long storage times are required, similar to case 1b. Indeed, these may be the processes responsible for the high U/Th of the ignimbrites. Relative importance of processes (1) and (2) is difficult to constrain, and both likely contributed. The finding of short transit times for mafic magma, in contrast to silicic magma that is long-lived or contains recycled components reinforces findings of Reagan et al. (2003) that silicic magma is more likely to stall than mafic magma. In the case of Parinacota, U/Th ratios in silicic rocks are more similar to ignimbrites than to metamorphic basement and thus constrain the depth of stagnation to the upper-most crust, i.e. in the shallow plumbing system immediately beneath the volcano.

5.4. Evolution of the volcanic plumbing system

We develop a conceptual model for the temporal development of the magma plumbing system bounded by the major events in the volcanic history (Fig. 7). Our aim is to show how the deep crustal signature permeates the system and that erupted composition is a result of the shifting mass balance from silicic (possibly largely recycled) upper-crustal to mafic lower-crustal components. For each time interval, we discuss the likely configuration and spatial

Table 2
Batch partial melting model results.[a,b]

Lithology	Bulk D_U	Bulk D_{Th}	Bulk D_U/D_{Th}	Modeled (^{230}Th/^{238}U) for degrees of partial melting below				
				1%	2%	5%	10%	20%
Belen mid-crust[c]	0.0029	0.00 13	2.23	1.142	1.075	1.030	1.014	1.006
Lower crust cumulates[d]	0.0130	0.0078	1.67	1.295	1.187	1.087	1.044	1.020
Spinel lherzolite (average[e])	0.0032	0.0018	1.78	1.068	1.036	1.015	1.007	1.003
Garnet lherzolite (average[e])	0.0027	0.0011	2.45	1.139	1.072	1.029	1.014	1.006

[a] Mineral abbreviations used below: ol = olivine, cpx = clinopyroxene, opx = orthopyroxene, gt = garnet, sp = spinel, amph = amphibole, mt = magnetite, biot = biotite, plag = plagioclase, qtz = quartz.
[b] Partition coefficients used: ol $D_U = 6\times10^{-5}$, $D_{Th} = 9.5\times10^{-6}$; opx $D_U = 0.0052$, $D_{Th} = 0.002$; sp $D_U = 0.007$ $D_{Th} = 0.0007$; amph $D_U = D_{Th} = 0.01$; mt $D_U = 0.04$ $D_{Th} = 0.004$ (Blundy and Wood, 2003); cpx $D_U = 0.023$ $D_{Th} = 0.019$ (Wood et al., 1999), gt $D_U = 0.013$ $D_{Th} = 0.0032$ (Elkins et al. 2008).
[c] biot 40%, qtz 25%, plag 25%, gt 5%, mt 5% (Wörner et al., 2000b).
[d] ol 25%, cpx 25%, gt 25%, amph 20%, mt 5%.
[e] Spinel lherzolite average modes: ol 80%, opx 10%, cpx 8%, sp 2%; garnet lherzolite average modes: ol 63%, opx 30%, gt 5%, cpx 2% (Maaløe and Aoki, 1977).

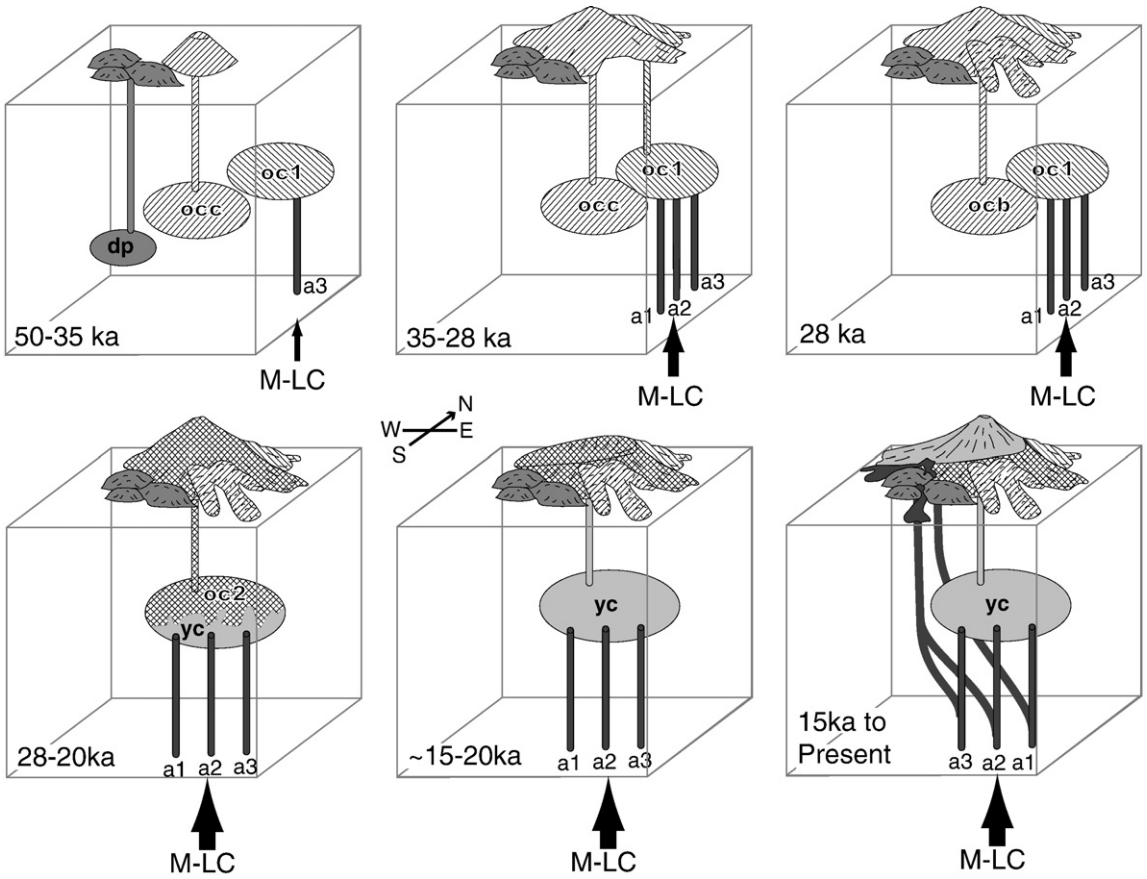

Fig. 7. Schematic step-by-step evolution of the upper-crustal magmatic system at Parinacota, and its surficial expression as volcanic edifice building, at time intervals indicated. Magma reservoirs are simplified as ellipsoids and pipes to emphasize inputs, outputs and connectivity among them. Lateral arrangement of reservoirs is partially constrained by vent locations, however vertical arrangement is constrained only as being deeper prior to disappearance of stable amphibole at onset of young cone growth. M-LC qualitatively represents flux from the mantle and lower crust into the upper-crustal volume shown.

arrangement of sub-volcanic reservoirs, the degree to which they operated as open or closed systems, and link changes in the magmatic system to morphology of the edifice.

5.4.1. Prior to 35 ka

During the early portion of old cone history, three texturally, chemically, and mineralogically distinct types of magma (*occ*, *dp* and *oc1* — Fig. 7), are grouped spatially — each built a sector of the edifice. They do not form clusters with respect to their age; rather each petrologic group yielded $^{40}Ar/^{39}Ar$ ages that span a large part of the interval between 52 and 35 ka, indicating that evolution in a single magma reservoir is unlikely. Moreover, uniformity in $^{87}Sr/^{86}Sr$ ratios within each group and disparity between groups suggests that these lavas represent contributions from three long-lived separate reservoirs (Fig. 7). Time-invariant $^{87}Sr/^{86}Sr$ ratios and increasing SiO_2 content of the southwest flank *dp* lavas with time (Fig. 3e–f), are consistent with fractional crystallization in an isolated magma reservoir. In contrast, the group with the highest $^{87}Sr/^{86}Sr$ ratios (*occ*) is nearly invariant with respect to $^{87}Sr/^{86}Sr$ ratios and SiO_2 contents (Fig. 3e–f), suggesting a steady-state system where heat input is balanced by cooling and heat removal by eruption.

North-flank (*oc1*) lavas have low $^{87}Sr/^{86}Sr$ ratios coupled with an increase in [Sr] with time, indicating that open-system recharge had occurred and that the admixed component was primarily a high-[Sr] basaltic andesite similar to *a3*. We interpret magma recharge to have affected the northern reservoir first, whereas the southern portions of the system (*occ* and *dp*) were not recharged at that time. Although eruption location provides some constraint on lateral arrangement of old cone magma bodies, their depth is constrained by the presence of amphibole, requiring pressures >100 MPa, or deeper than 3 km (Rutherford and Hill, 1993). Narrow oxide rims on amphibole phenocrysts suggest rapid ascent from amphibole-stable pressures.

5.4.2. 35–28 ka

Lavas from a brief period of increased flux between 31 and 28 ka (*ocb*) have indistinguishable $^{87}Sr/^{86}Sr$ ratios from the *occ* lavas in the previous time interval (Fig. 3f), and have the same phenocryst inventory, although crystals in *ocb* are larger, with, for example, sanidine crystals up to 1 cm. Based on the similarities in isotopic compositions and phenocryst assemblage, we interpret a genetic link between the thermally buffered *occ* reservoir and younger *ocb* lavas (Fig. 7). The other lavas erupted in this time interval (*oc1a*) have variable texture, mineralogy, and $^{87}Sr/^{86}Sr$ ratios that are different from those of any previous magma batch (Fig. 3f). Their near-secular equilibrium ($^{230}Th/^{238}U$) ratios and intermediate $^{87}Sr/^{86}Sr$ ratios are similar to *a1*. These data are permissive of either recharge of the northern reservoir by a mafic magma that had already incorporated mid- to upper-crustal melts (*a1*), or wall-rock contamination along the margin of the *oc1* reservoir that occurred after recharge by lower-crustal magma *a3*.

5.4.3. 28–20 ka

We interpret the large amount of scatter in chemical and isotopic compositions during this time period to reflect frequent recharge, corroborating phenocryst zoning observations (Ginibre and Wörner, 2007). It is likely that consolidation of three infrequently recharged sub-reservoirs that were active from 52 to 35 ka occurred, two of which were extant by the time of border dacite eruptions. We suggest

that increased recharge led to development of a single magma reservoir. Such coalescence of small isolated magma batches by increased recharge has also been postulated for other volcanic centers, e.g. the 39 ka Campanian Ignimbrite and the 15 ka Neapolitan Yellow Tuff in Italy (Pabst et al., 2008).

5.4.4. Sector collapse

A bomb deposited on top of old cone lavas yielded a $^{40}Ar/^{39}Ar$ age of 22.4 ± 7.5 ka and is within error of the estimated time of sector collapse (constrained to ~15–20 ky, Hora et al., 2007). This bomb has a relatively mafic composition, and $^{87}Sr/^{86}Sr$ and ($^{230}Th/^{232}Th$) ratios that are similar to young cone lavas. Its composition indicates that by the time of sector collapse, magma recharge had already changed the magmatic system to a composition indistinguishable from young cone lavas. In most other volcanoes that have been studied in similar detail (Pallister et al., 1992; Morgan et al., 2006; Wark et al., 2007), recharge is interpreted to trigger large eruptions within tens to hundreds of years. In contrast to these, the Parinacota data suggest a significantly more protracted recharge interval of ~30 ka, and no ensuing climactic eruption.

5.4.5. 15 ka to present

Two clusters of ($^{230}Th/^{238}U$) ratios in young cone samples indicate a variable mid- to upper-crustal overprint of magmas that previously interacted with garnet-bearing lower crust. The cluster that is similar to flank eruption *a3* is interpreted to have a minimal shallow crust overprint, whereas the cluster that is similar to flank eruption *a1* likely reflects more shallow crustal assimilation. Symmetry of the young cone edifice indicates that the bulk of the magma erupted from the same shallow conduit. While relatively uniform young cone lavas were exclusively erupted from the central vent, chemical and isotopic heterogeneity increases with distance from the summit. Despite broadly similar major-element compositions and eruption from the same low-elevation flank vent within 1 ka of one another, Ajata lavas *a2* and *a3* represent nearly the entire range of ($^{230}Th/^{232}Th$) and ($^{230}Th/^{238}U$) and a significant portion of the $^{87}Sr/^{86}Sr$ range found at Parinacota. We suggest that these magmas remained distinct because they bypassed the main reservoir and thereby avoided mixing with a larger volume of stored magma. They may represent heterogeneity of inputs from the lower crust that were otherwise involved in mafic recharge. Whereas *a2* incorporated xenocrysts from the dome plateau through which it erupted, *a3* shows little interaction with dome plateau rocks or the *a2* magma that preceded it.

5.5. Transition from calc-alkaline to near-tholeiitic magmas as a function of magma throughput and self-insulation of the conduit system

A decrease in CA/TH index (Fig. 3a) occurred between the time of border dacite eruption (28 ka) and sector collapse (~15–20 ka, Hora et al., 2007). This change is interpreted to coincide with reorganization of the magma system from a multi-reservoir system to a single reservoir, a decrease in magma transit time through the crustal column, and increased throughput of magma. The shallow magma system is envisioned to have modified inputs from the lower crust via low-pressure fractional crystallization, magma mixing, and assimilation. All of these processes would overprint lower-crustal chemical signatures, and assimilation and mixing can change isotopic ratios. The amount of overprinting is expected to be dependent on magma residence time and temperature contrast: as shallow residence time increases, so does the likelihood of assimilation and incorporation of remobilized crystals, leading to more phenocryst-rich and porphyritic textures. A decrease in the MASH-to-surface transit time minimized the effects of shallow overprinting as the system evolved from low- to high-magma fluxes. Formation of crystal cumulates produced by early magmas is envisioned to have self-insulated the plumbing system, which decreased the likelihood of subsequent assimilation of host rock, particularly if magma transit time through the crust was reduced. Conduit self-insulation is expected to move overall magma composition from calc-alkaline to tholeiitic affinities, as it decreases the efficiency with which magma can assimilate shallow wall-rock. The relative importance of self-insulation and increased magma flux are not resolvable at Parinacota. However, sparse data from four migrating volcanic centers in Central America suggest analogous age progression from old, slow, silicic, and calc-alkaline to young, fast, mafic, and tholeiitic (Halsor and Rose, 1988). These observations indicate that either the zone of self-insulation extends to distances similar to the 5 km displacement between old and young vents, or that it is subordinate to the effect of increased throughput.

6. Conclusions

Change from upper- to lower-crustal magma characteristics in the Parinacota system was a result of both an increase in throughput (recharge and eruption rates increased), and a decrease in transit times from the lower crust to the surface. The initial state of the system was a highly compartmentalized shallow reservoir, in which long storage and crystallization times and significant assimilation of secular equilibrium material resulted in crust-like ($^{230}Th/^{232}Th$). The final state was a simpler system in which increased recharge was balanced by high eruption rates. Increased recharge frequency initiated consolidation of reservoirs, which did not affect all parts of the system simultaneously, and took ~15 ka to complete. A remaining problem is determining how output from the MASH zone is modulated, affecting flux through the crust, rate of ascent, and frequency of recharge. Because crustal structure and stress regime are likely invariant on timescales comparable to edifice building, and pressure effects of the edifice itself decrease significantly with depth, neither can affect output from the lower crust. Some possibilities are that separation of buoyant melt bodies may proceed sporadically, or that variability in MASH output mirrors changes in lower-crustal input of mantle melts.

Slow and fast magma throughput regimes have been well documented separately in the Central Andes based on volcano histories and ranges of magma composition. As a general rule, relatively short-lived volcanic systems (<0.3 Ma) have symmetrical cones of largely mafic andesite compositions (Wörner et al., 2000a). Longer-lived magma systems (up to several Ma) can be much more diverse in magma composition and morphology (Klemetti and Grunder, 2008) or represented by monotonous dacite dome complexes with compositions similar to parts of the old cone of Parinacota (e.g. Taapaca, Clavero et al., 2004). Our data from Parinacota illustrate how changes from one magmatic regime to the other take place, how fast such transitions may be, and what their textural, chemical, and isotopic consequences are.

We show that a 'dirty' to 'clean' transition is a viable mechanism for generating differentiation trends that straddle the calc-alkaline vs. tholeiitic compositional boundary. Elevated LREE/HREE and large Th-excess in the most tholeiitic samples suggest both are controlled by garnet-residual processes in the lower crust whereas upper-crustal assimilation exerts significant control on melt FeO*/MgO. Apparent calc-alkaline or tholeiitic affinity at Parinacota is apparently due to mixing among magmas sourced in the upper- and lower-crust, respectively. Transit times are constrained by ^{238}U–^{230}Th disequilibria to be shortest for the least calc-alkaline samples, indicating that the deep crustal signature had been preserved. Long upper-crustal stagnation times, evinced by near-equiline, upper-crustal ($^{230}Th/^{232}Th$) are correlated with the most contaminated, calc-alkaline samples. Arc magmas traverse thick continental crust at variable speeds, dependent largely on throughput and whether shallow stagnation occurs in sub-volcanic systems. Our results illustrate the importance of shallow processes in modifying or damping deep crustal heterogeneities in parent magma compositions. A significant

amount of the chemical and isotopic variability observed in these settings may therefore depend on the degree to which shallow and deep processes have affected magma composition.

Acknowledgements

We thank Jorge Clavero for sharing his knowledge and previous mapping that facilitated fieldwork at Parinacota as well as Carlos Nassar and CONAF for permission to work and sample in Parque Nacional Lauca. This work was supported by U.S. National Science Foundation (NSF) grants EAR-0337667, EAR-0516760, and EAR-0738007 to Singer, Geological Society of America (GSA) and Sigma Xi grants to Hora, and German Science Foundation grants Wo362/18 and Wo236/20 to Wörner. We would thank editor Richard Carlson for efficient handling of this submission, and Mary Reid and an anonymous reviewer for thoughtful comments that greatly improved this manuscript.

Appendix A. Supplementary data

Supplementary data associated with this article can be found in the online version, at doi:10.1016/j.epsl.2009.05.042.

References

Aitcheson, S.J., Harmon, R.S., Moorbath, S., Schneider, A., Soler, P., Soria-Escalante, E., Steele, G., Swainbank, I., Wörner, G., 1995. Pb isotopes define basement domains of the Altiplano, central Andes. Geology 23 (6), 555–558.

Allegre, C.J., Condomines, M., 1982. Basalt genesis and mantle structure studied through Th-isotopic geochemistry. Nature 299 (5878), 21–24.

Allmendinger, R.W., Jordan, T.E., Kay, S.M., Isacks, B.L., 1997. The evolution of the Altiplano–Puna plateau of the central Andes. Annu. Rev. Earth Planet. Sci. 25, 139–174.

Annen, C., Blundy, J.D., Sparks, R.S.J., 2006. The genesis of intermediate and silicic magmas in deep crustal hot zones. J. Petrol. 47 (3), 505–539.

Arculus, R.J., 2003. Use and abuse of the terms calcalkaline and calcalkalic. J. Petrol. 44 (5), 929–935.

Beck, S.L., Zandt, G., Myers, S.C., Wallace, T.C., Silver, P.G., Drake, L., 1996. Crustal-thickness variations in the central Andes. Geology 24 (5), 407–410.

Blundy, J., Wood, B., 2003. Mineral-melt partitioning of uranium, thorium and their daughters. In: Bourdon, B., Henderson, G.M., Lundstrom, C.C., Turner, S.P. (Eds.), Uranium Series Geochemistry. Reviews in Mineralogy and Geochemistry, vol. 52. Mineralogical Society of America, pp. 59–123.

Bourdon, B., Wörner, G., Zindler, A., 2000. U-series evidence for crustal involvement and magma residence times in the petrogenesis of Parinacota Volcano, Chile. Contrib. Mineral. Petrol. 139 (4), 458–469.

Cheng, H., Edwards, R.L., Hoff, J., Gallup, C.D., Richards, D.A., Asmerom, Y., 2000. The half-lives of Uranium-234 and Thorium-230. Chem. Geol. 169 (1-2), 17–33.

Clavero, J.E., Sparks, R.S.J., Huppert, H.E., 2002. Geological constraints on the emplacement mechanism of the Parinacota debris avalanche, northern Chile. Bull. Volcanol. 64 (1), 40–54.

Clavero, J.E., Sparks, R.S.J., Pringle, M.S., Polanco, E., Gardeweg, M.C., 2004. Evolution and volcanic hazards of Taapaca Volcanic Complex, central Andes of northern Chile. J. Geol. Soc. 161, 603–618.

Coulon, C., Thorpe, R.S., 1981. Role of continental crust in petrogenesis of orogenic volcanic associations. Tectonophysics 77 (1–2), 79–93.

Davidson, J.P., McMillan, N.J., Moorbath, S., Wörner, G., Harmon, R.S., Lopez-Escobar, L., 1990. The Nevados de Payachata volcanic region (18°S 69°W, N Chile) II. evidence for widespread crustal involvement in Andean magmatism. Contrib. Mineral. Petrol. 105 (4), 412–432.

Davidson, J., Turner, S., Handley, H., Macpherson, C., Dosseto, A., 2007. Amphibole "sponge" in arc crust? Geology 35 (9), 787–790.

Elkins, L.J., Gaetani, G.A., Sims, K.W.W., 2008. Partitioning of U and Th during garnet pyroxenite partial melting: constraints on the source of alkaline ocean island basalts. Earth Planet. Sci. Lett. 265 (1–2), 270–286.

Entenmann, 1994. Magmatic evolution of the Nevados de Payachata complex and the petrogenesis of basaltic andesites in the Central Volcanic Zone of northern Chile [Ph.D. thesis]: Johannes Gutenberg-Universität in Mainz, 188 p.

Garrison, J., Davidson, J., Reid, M., Turner, S., 2006. Source versus differentiation controls on U-series disequilibria: insights from Cotopaxi Volcano, Ecuador. Earth Planet. Sci. Lett. 244 (3–4), 548–565.

George, R., Turner, S., Hawkesworth, C., Bacon, C.R., Nye, C., Stelling, P., Dreher, S., 2004. Chemical versus temporal controls on the evolution of tholeiitic and calc-alkaline magmas at two volcanoes in the Alaska–Aleutian arc. J. Petrol. 45 (1), 203–219.

Ginibre, C., Wörner, G., 2007. Variable parent magmas and recharge regimes of the Parinacota magma system (N. Chile) revealed by Fe, Mg and Sr zoning in plagioclase. Lithos 98 (1–4), 118–140.

Ginibre, C., Worner, G., Kronz, A., 2002. Minor- and trace-element zoning in plagioclase: implications for magma chamber processes at Parinacota Volcano, Northern Chile. Contrib. Mineral. Petrol. 143 (3), 300–315.

Grove, T.L., Baker, M.B., 1984. Phase-equilibrium controls on the tholeiitic versus calc-alkaline differentiation trends. J. Geophys. Res. 89 (NB5), 3253–3274.

Grove, T.L., Kinzler, R.J., 1986. Petrogenesis of andesites. Annu. Rev. Earth Planet. Sci. 14, 417–454.

Halsor, S.P., Rose, W.I., 1988. Common characteristics of paired volcanoes in northern Central America. J. Geophys. Res.–Solid Earth Planets 93 (B5), 4467–4476.

Hildreth, W., Moorbath, S., 1988. Crustal contributions to arc magmatism in the Andes of central Chile. Contrib. Mineral. Petrol. 98 (4), 455–489.

Hora, J.M., Singer, B.S., Wörner, G., 2007. Volcano evolution and eruptive flux on the thick crust of the Andean Central Volcanic Zone; $^{40}Ar/^{39}Ar$ constraints from Volcán Parinacota, Chile. Geol. Soc. Am. Bull. 119 (3–4), 343–362.

Jicha, B.R., Johnson, C.M., Hildreth, W., Beard, B.L., Hart, G.L., Shirey, S.B., Singer, B.S., 2009. Discriminating assimilants and decoupling deep- vs. shallow-level crystal records at Mount Adams using ^{238}U–^{230}Th disequilibria and Os isotopes. Earth Planet. Sci. Lett. 277 (1–2), 38–49.

Jicha, B.R., Singer, B.S., Beard, B.L., Johnson, C.M., 2005. Contrasting timescales of crystallization and magma storage beneath the Aleutian island arc. Earth Planet. Sci. Lett. 236 (1–2), 195–210.

Kay, S.M., Kay, R.W., Citron, G.P., 1982. Tectonic controls on tholeiitic and calc-alkaline magmatism in the Aleutian arc. J. Geophys. Res. 87 (NB5), 4051–4072.

Kay, S.M., Mpodozis, C., Coira, B., 1999. Neogene magmatism, tectonism, and mineral deposits of the central Andes (22° to 33° S Latitude). In: Skinner, B. (Ed.), Geology and Ore Deposits of the Central Andes: Society of Economic Geologists Special Publication, pp. 27–59.

Kersting, A.B., Arculus, R.J., Gust, D.A., 1996. Lithospheric contributions to arc magmatism: isotope variations along strike in volcanoes of Honshu, Japan. Science 272 (5267), 1464–1468.

Klemetti, E.W., Grunder, A.L., 2008. Volcanic evolution of Volcan Aucanquilcha: a long-lived dacite volcano in the central Andes of Northern Chile. Bull. Volcanol. 70 (5), 633–650.

Lee, C.T.A., Cheng, X., Horodyskyj, U., 2006. The development and refinement of continental arcs by primary basaltic magmatism, garnet pyroxenite accumulation, basaltic recharge and delamination: insights from the Sierra Nevada, California. Contrib. Mineral. Petrol. 151 (2), 222–242.

Leeman, W.P., 1983. The influence of crustal structure on compositions of subduction-related magmas. J. Volcanol. Geotherm. Res. 18 (1–4), 561–588.

Maaløe, S., Aoki, K.I., 1977. Major element composition of upper mantle estimated from composition of lherzolites. Contrib. Mineral. Petrol. 63 (2), 161–173.

Macpherson, C.G., 2008. Lithosphere erosion and crustal growth in subduction zones: insights from initiation of the nascent East Philippine Arc. Geology 36 (4), 311–314.

Macpherson, C.G., Dreher, S.T., Thirlwall, M.F., 2006. Adakites without slab melting: high pressure differentiation of island arc magma, Mindanao, the Philippines. Earth Planet. Sci. Lett. 243 (3–4), 581–593.

Mamani, M., Tassara, A., Wörner, G., 2008. Composition and structural control of crustal domains in the central Andes. Geochem. Geophys. Geosyst. 9 (3) (Q03006).

Mamani, M., Wörner, G., Semperé, T., in press. Geochemical variations in igneous rocks of the Central Andean Orocline (13° to 18°S): tracing crustal thickening and magma generation through time and space. Geol. Soc. Am. Bull. doi:10.1130/B26538.1

Miyashiro, A., 1974. Volcanic rock series in island arcs and active continental margins. Am. J. Sci. 274 (4), 321–355.

Morgan, D.J., Blake, S., Rogers, N.W., De Vivo, B., Rolandi, G., Davidson, J.P., 2006. Magma chamber recharge at Vesuvius in the century prior to the eruption of AD 79. Geology 34 (10), 845–848.

Muntener, O., Kelemen, P.B., Grove, T.L., 2001. The role of H_2O during crystallization of primitive arc magmas under uppermost mantle conditions and genesis of igneous pyroxenites: an experimental study. Contrib. Mineral. Petrol. 141 (6), 643–658.

Myers, J.D., Marsh, B.D., Sinha, A.K., 1985. Strontium isotopic and selected trace-element variations between 2 Aleutian volcanic centers (Adak and Atka) — implications for the development of arc volcanic plumbing systems. Contrib. Mineral. Petrol. 91 (3), 221–234.

Pabst, S., Worner, G., Civetta, L., Tesoro, R., 2008. Magma chamber evolution prior to the Campanian Ignimbrite and Neapolitan Yellow Tuff eruptions (Campi Flegrei, Italy). Bull. Volcanol. 70 (8), 961–976.

Pallister, J.S., Hoblitt, R.P., Reyes, A.G., 1992. A basalt trigger for the 1991 eruptions of Pinatubo Volcano. Nature 356 (6368), 426–428.

Pertermann, M., Hirschmann, M.M., Hametner, K., Gunther, D., Schmidt, M.W., 2004. Experimental determination of trace element partitioning between garnet and silica-rich liquid during anhydrous partial melting of MORB-like eclogite. Geochem. Geophys. Geosyst. 5.

Portnyagin, M., Manea, V.C., 2008. Mantle temperature control on composition of arc magmas along the Central Kamchatka Depression. Geology 36 (7), 519–522.

Ramos, V.A., 2008. The basement of the Central Andes: the Arequipa and related terranes. Annu. Rev. Earth Planet. Sci. 36, 289–324.

Reagan, M.K., Sims, K.W.W., Erich, J., Thomas, R.B., Cheng, H., Edwards, R.L., Layne, G., Ball, L., 2003. Time-scales of differentiation from mafic parents to rhyolite in North American continental arcs. J. Petrol. 44 (9), 1703–1726.

Robinson, J.A.C., Wood, B.J., 1998. The depth of the spinel to garnet transition at the peridotite solidus. Earth Planet. Sci. Lett. 164, 277–284.

Rutherford, M.J., Hill, P.M., 1993. Magma ascent rates from amphibole breakdown — an experimental study applied to the 1980–1986 Mount St. Helens eruptions. J. Geophys. Res.–Solid Earth 98 (B11), 19667–19685.

Singer, B.S., Jicha, B.R., Harper, M.A., Naranjo, J.A., Lara, L.E., Moreno-Roa, H., 2008. Eruptive history, geochronology, and magmatic evolution of the Puyehue–Cordon Caulle volcanic complex, Chile. Geol. Soc. Am. Bull. 120 (5–6), 599–618.

Sisson, T.W., Grove, T.L., 1993. Experimental investigations of the role of H_2O in calc-alkaline differentiation and subduction zone magmatism. Contrib. Mineral. Petrol. 113 (2), 143–166.

Tormey, D.R., Hickey-Vargas, R., Frey, F.A., López-Escobar, L., 1991. Recent lavas from the Andean volcanic front (33 to 42°S); interpretations of along-arc compositional variations. In: Harmon, R.S., Rapela, C.W. (Eds.), Andean Magmatism and its Tectonic Setting: Special Paper. Geological Society of America, Boulder, Colorado, pp. 57–77.

Turner, S., Evans, P., Hawkesworth, C., 2001. Ultrafast source-to-surface movement of melt at island arcs from ^{226}Ra–^{230}Th systematics. Science 292 (5520), 1363–1366.

Turner, S.P., Bourdon, B., Gill, J., 2003. Insights into magma genesis at convergent margins from U-series isotopes. In: Bourdon, B., Henderson, G.M., Lundstrom, C.C., Turner, S.P. (Eds.), Uranium-Series Geochemistry: Reviews in Mineralogy and Geochemistry. Mineralogical Society of America, pp. 255–316.

van Westrenen, W., Blundy, J., Wood, B., 1999. Crystal-chemical controls on trace element partitioning between garnet and anhydrous silicate melt. Am. Mineral. 84 (5–6), 838–847.

Wark, D.A., Hildreth, W., Spear, F.S., Cherniak, D.J., Watson, E.B., 2007. Pre-eruption recharge of the Bishop magma system. Geology 35 (3), 235–238.

Williams, R.W., Gill, J.B., 1989. Effects of partial melting on the uranium decay series. Geochim. Cosmochim. Acta 53 (7), 1607–1619.

Wood, B.J., Blundy, J.D., Robinson, J.A.C., 1999. The role of clinopyroxene in generating U-series disequilibrium during mantle melting. Geochim. Cosmochim. Acta 63 (10), 1613–1620.

Wörner, G., Hammerschmidt, K., Henjes-Kunst, F., Lezaun, J., Wilke, H., 2000a. Geochronology (^{40}Ar/^{39}Ar, K–Ar and He-exposure ages) of Cenozoic magmatic rocks from northern Chile (18–22° S): implications for magmatism and tectonic evolution of the central Andes. Rev. Geol. Chile 27 (2), 205–240.

Wörner, G., Harmon, R.S., Davidson, J., Moorbath, S., Turner, D.L., Mcmillan, N., Nye, C., Lopez-Escobar, L., Moreno, H., 1988. The Nevados de Payachata volcanic region (18°S/69°W, N. Chile) I. Geological, geochemical, and isotopic observations. Bull. Volcanol. 50 (5), 287–303.

Wörner, G., Lezaun, J., Beck, A., Heber, V., Lucassen, F., Zinngrebe, E., Rossling, R., Wilke, H.G., 2000b. Precambrian and Early Paleozoic evolution of the Andean basement at Belen (northern Chile) and Cerro Uyarani (western Bolivia Altiplano). J. South Am. Earth Sci. 13 (8), 717–737.

Wörner, G., Moorbath, S., Harmon, R.S., 1992. Andean Cenozoic volcanic centers reflect basement isotopic domains. Geology 20 (12), 1103–1106.

Yuan, X., Sobolev, S.V., Kind, R., 2002. Moho topography in the central Andes and its geodynamic implications. Earth Planet. Sci. Lett. 199 (3–4), 389–402.

Zou, H.B., Zindler, A., 2000. Theoretical studies of ^{238}U–^{230}Th–^{226}Ra and ^{235}U–^{231}Pa disequilibria in young lavas produced by mantle melting. Geochim. Cosmochim. Acta 64 (10), 1809–1817.